21st Australasian Fluid Mechanics Conference
Adelaide, Australia
10-13 December 2018

An experimental investigation into the breakdown of riblet drag reduction at post-optimal conditions

R. Newton, D. Chung and N. Hutchins

Department of Mechanical Engineering, University of Melbourne, Victoria 3010, Australia

Abstract

A long-standing question in riblet research is why drag reduction only occurs within a small, non-dimensionally scaled envelope, outside of which drag is significantly increased. For riblets with viscous-scaled spacings that are much larger than those required for drag reduction, one hypothesis is that the riblets exhibit *k*-type, 'fully rough' behaviour. However, this seems counter-intuitive since fully rough behaviour is typically associated with a dominance of pressure drag over viscous drag, and yet riblets can sustain no pressure drag.

This study aims to investigate this issue by conducting single normal hot-wire traverses above a trapezoidal riblet surface, over a range of drag-increasing viscous-scaled riblet spacings. Novelty was added by also measuring within the riblet valleys, providing a unique look at the turbulent behaviour within them.

Previously proposed mechanisms for the breakdown in drag reduction have included lodgement of turbulence within the riblet valleys, and the development of a Kelvin–Helmholtz instability, but neither mechanism appears active in our results. They instead show a reduction in turbulent energy as riblet spacing increases, despite a significant increase in drag, which does seem to be approaching a *k*-type roughness asymptote as hypothesised. This may be caused by the generation of time-invariant secondary flows above the riblet tips and corners of the riblet valleys, although this will require further investigation.

Introduction

For a typical airliner, around 50% of the total drag acting during cruise is due to skin friction [1]. This means that a large proportion of the fuel expended, and resultant emissions produced, are purely to overcome this friction. With 37 million flights worldwide in 2017 [2], and this number expected to double over the next twenty years [3], even small reductions in drag would provide appreciable economic and environmental benefits.

To minimise skin friction, it has long been our intuition to make a fluid-bounded surface as smooth as possible, but this belief came under scrutiny following observations of the skin topology of fast-swimming sharks. Researchers found that the scales of these sharks contained a unique, but regular three-dimensional structure, with micro-scale ridges that run parallel with the shark's body. Aerodynamicists soon picked up on this [4], and by modelling the skin as a series of regularly spaced fins, known as riblets, they were able to determine that the riblets could reduce skin friction drag even beyond that of any smooth surface; with both experimental and numerical studies achieving skin friction reductions (*DR*, defined as a change in friction coefficient c_f with respect to a smooth wall c_{f_0}) ranging from 7–10% [5], when the viscous-scaled riblet spacing ($s^+ = sU_\tau/\nu$) is 16–20 and the riblet height-to-spacing ratio (h/s) is 0.5–0.7. Here s is the riblet spacing, $U_\tau = \sqrt{\tau_w/\rho}$ is the wall friction velocity (where τ_w is the wall shear stress and ρ is the fluid density), ν is kinematic viscosity and h is the riblet height.

However, despite the excitement generated by these results and subsequent studies of notable depth, e.g. Bechert *et al.* (1997) [5], no commercial aircraft to date are installed with riblets. One possible cause for this is that in-flight testing has so far suggested that a maximum *DR* of just 2% may be achievable in practice, contrary to laboratory predictions. This reduced effectiveness results from many factors including imperfect alignment of the riblets with the flow direction, incomplete coverage of wetted surfaces, and the fact that there is a strong friction Reynolds number ($Re_\tau = \delta_{99}U_\tau/\nu$, δ_{99} is the 99% boundary layer thickness) dependence in the attainable *DR* [6].

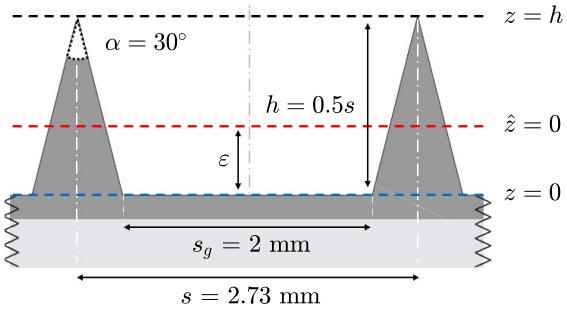

Figure 1: Cross-sectional sketch of the manufactured riblet. s is the riblet spacing, s_g is the riblet valley spacing, h is the riblet height and α is the blade angle. The blue dashed line shows the base of the riblet valley ($z = 0$), the red dashed line shows the position of the virtual origin ($\hat{z} = 0$) and the black dashed line indicates the position of the riblet crests ($z = h$).

The mechanism of how optimally scaled (s^+_{opt}) riblets reduce drag is well understood, as the riblets impede the movement of quasi-streamwise vortices, constraining them above the riblet valleys, which limits the turbulent momentum transfer close to the surface and in the valleys [7]. But for non-optimally scaled riblets the picture is less clear. For riblet spacings that are smaller than optimal, *DR* is theoretically proportional to the difference in viscous-scaled protrusion height (Δh^+), between the origins of the streamwise and spanwise flow [8]. However this no longer holds for riblets larger than optimal, owing to an increasing influence of Reynolds stresses. A prevailing theory for this 'breakdown' was first described by Choi *et al.* in 1993 [7], who state that the breakdown coincides with the lodging of the quasi-streamwise vortices within the riblet grooves. This would increase drag, as the previous fluid interaction of the vortices above the riblet tips and low velocity quasi-laminar fluid in the grooves, would be replaced by a typical wall interaction, where the riblet wall has a greater surface area than the smooth.

A further theory was documented in 2011 by García–Mayoral & Jiménez [9], who conducted a series of direct numerical simulations with riblet sizes ranging from drag reducing to drag increasing. They found that for riblet sizes close to the point of breakdown of drag reduction, a series of near-wall spanwise vortex rollers formed with a riblet size-dependent intensity, similar in structure to a Kelvin–Helmholtz (K–H) instability.

Case	Symbol	U_∞ (m/s)	ν (m^2/s)	δ_{99} (m)	ε (m)	U_τ (m/s)	ΔU^+	Re_τ	s^+	l^+
5R	●	5.07	1.56×10^{-5}	0.0780	0.00113	0.228	2.526	1132	39.8	14.58
7R	●	7.47	1.53×10^{-5}	0.0712	0.00108	0.348	4.438	1620	62.3	22.82
10R	●	10.04	1.55×10^{-5}	0.0743	0.00100	0.511	6.743	2450	90.1	33.00
15R	●	14.86	1.51×10^{-5}	0.0673	0.00072	0.809	8.911	3611	146.0	53.47
20R	●	19.87	1.52×10^{-5}	0.0707	0.00058	1.117	9.955	5179	201.0	73.61
25R	●	24.95	1.54×10^{-5}	0.0702	0.00076	1.390	10.25	6354	247.0	90.48
30R	●	30.12	1.54×10^{-5}	0.0691	0.00080	1.688	10.70	7551	298.3	109.26

Table 1: Complete summary of experiment results. U_∞ is the Pitot tube measured free-stream velocity, ν is the kinematic viscosity, δ_{99} is the 99% boundary layer thickness, ε is the virtual origin offset, U_τ is the friction velocity, ΔU^+ is the Hama roughness function, Re_τ is the friction Reynolds number ($Re_\tau = \delta_{99}U_\tau/\nu$), s^+ and l^+ are the viscous-scaled riblet spacing and hot-wire length i.e. $l^+ = lU_\tau/\nu$.

This was determined from spectral analysis, where very wide ($\lambda_y^+ = \lambda_y U_\tau/\nu > 100$, λ_y is the spanwise wavelength), large-scale energy with a streamwise wavelength of $\lambda_x^+ \approx 150$ appears beyond the point of breakdown.

For riblets scaled far beyond the point of breakdown ($s^+ \gg s_{opt}, DR > 0$) it is generally accepted that the relationship between DR and s^+ asymptotes to the fully rough behaviour of so-called k-type roughness [4, 9]. This is counter-intuitive because fully rough behaviour is typically associated with a dominance of pressure drag over viscous drag [10], and riblets present no streamwise component of surface normals upon which this pressure drag could act. Under this limitation, only a finite maximum drag increase is logical, and as such the turbulence may be expected to revert towards a smooth wall state at very high s^+, but with the addition of increased surface area. Despite the issues with this hypothesis, no practical (see [4]) riblet surface has been analysed at $s^+ > 40$. Although such geometries may not appear to be of interest in terms of drag reduction, analysis could provide further insight on how the proposed K–H instability develops, and if this structure can be suppressed. Additionally, it would confirm if there is increasing turbulence in the riblet valleys at high s^+ and this could subsequently inform more meaningful riblet designs.

Experiment Method

To investigate this regime where $s^+ \gg s_{opt}^+, DR > 0$, a series of zero pressure gradient wall-normal traverses with a single boundary layer hot-wire probe have been conducted above a trapezoidal riblet surface, using the 6.7 × 0.94 × 0.38 m Adjustable Pressure Gradient Boundary Layer Wind Tunnel facility (APGBLWT) at the University of Melbourne. Traverses differed by adjusting the free-stream velocity (U_∞) from 5 m/s – 30 m/s, and all measurements were taken along the centreline (y = 0.47 m) of the working section at a fixed streamwise position x = 4 m downstream of the inlet's sandpaper trip, ensuring a fully developed boundary layer. The maximum free stream turbulence level at the measurement station was $\leq 0.2\%$.

The dimensions of the riblet (figure 1) were chosen to match that which was previously analysed by Bechert *et al.* [5]; a surface that achieved a maximum DR of 8.2% with a blade angle (α) of 30° and h/s of 0.5. An s of 2.73 mm was selected, which corresponds to a riblet valley spacing (s_g) of 2 mm. This size permits us to traverse the hot-wire probe into the riblet valleys, with minimal clearance between the probe and valley side walls.

The riblet surface was manufactured in-house using a tile duplication method. This involved machining a master tile from PVC using a three-axis CNC router in combination with a custom cutting tool; using it to mould a silastomer negative of the tile, and then using the negative to cast the 30 riblet-engraved polyurethane tiles required to cover the 6.7 × 0.94 m working section floor, in a 10 × 3 formation.

The probe sensor diameter (d) was 5 µm and the sensor length (l) was etched to 1 mm. This is important as the free-stream velocity is adjusted to alter s^+, and so the non-dimensional wire length l^+ also varied between experiments. This has implications on spatial resolution, and should be considered when examining the results presented, as the highest s^+ cases yield an $l^+ > 100$, which according to Hutchins *et al.* (2009) [11] can cause substantial spatial attenuation and a spurious reduction of the near wall turbulence intensity peak.

Experiment Results

Table 1 provides a complete summary of results from the seven different experimental setups. To plot the data on a typical logarithmic axis, all z-positions have been adjusted to a datum centred at the base of the riblet valley ($z = 0$, figure 1). A virtual origin adjusted position is denoted as $\hat{z} = z - \varepsilon$, where ε was found by a log region fitting technique, which was also used to the find the friction velocity (U_τ) and Hama roughness function (ΔU^+) for each case studied. By the nature of calculation, ε also contains a certain amount of z-positional error, which may contribute to its fluctuating value in table 1.

Velocity profiles and Hama roughness function

Figure 2(a) shows the inner-scaled mean velocity profiles above the riblets for all experimental cases. In general, there is a clear decrease in maximum U^+, indicating a drag increase with respect to the smooth wall. This trend is clear for $39.8 \leq s^+ \leq 146.0$, although a convergence of the profiles to a fixed value of $U_\infty^+ = 17.8$ in the wake region can be seen for $s^+ \geq 201.0$. This indicates (since $U_\infty^+ = \sqrt{2/c_f}$) that the friction coefficient of the riblet surface becomes constant at high s^+, which is a condition of the fully rough regime.

In addition, we know that for a developing boundary layer that is exhibiting fully rough behaviour, we would also expect k_s/δ_{99} to become constant [13]. Hence by plotting U^+ vs. $\hat{z}/k_s$; a collapse in the fully rough regime is expected, and is indeed demonstrated in figure 2(b) with a collapse for the highest s^+ cases. Interestingly, the collapse is also seen below the riblet crests (position denoted by ○) for $s^+ \geq 247.0$, which has not typically been the case for other fully rough geometries within the roughness canopy [14].

In figure 2(c) an equivalent sand grain roughness is extracted for the riblet surface by forcing the results for ΔU^+ vs. k_s^+ onto Nikuradse's fully rough asymptote ($\Delta U^+ = \kappa^{-1}\log(k_s^+) + A - B$) where κ = 0.384, A = 4.17 and B = 8.5 [15]. Note that the highest Re_τ case is used to find this, which effectively forces this point onto the asymptote, although cases $20R$ – $30R$ all provide a sandgrain roughness of 2.94 ± 0.1 mm, meaning that $k_s/h \approx 2.15$. Together, figures 2(a–c) prove that k-type fully rough behaviour, does indeed occur for $s^+ \geq 201.0$, along with a sizable increase in drag up to $s^+ = 298.3$.

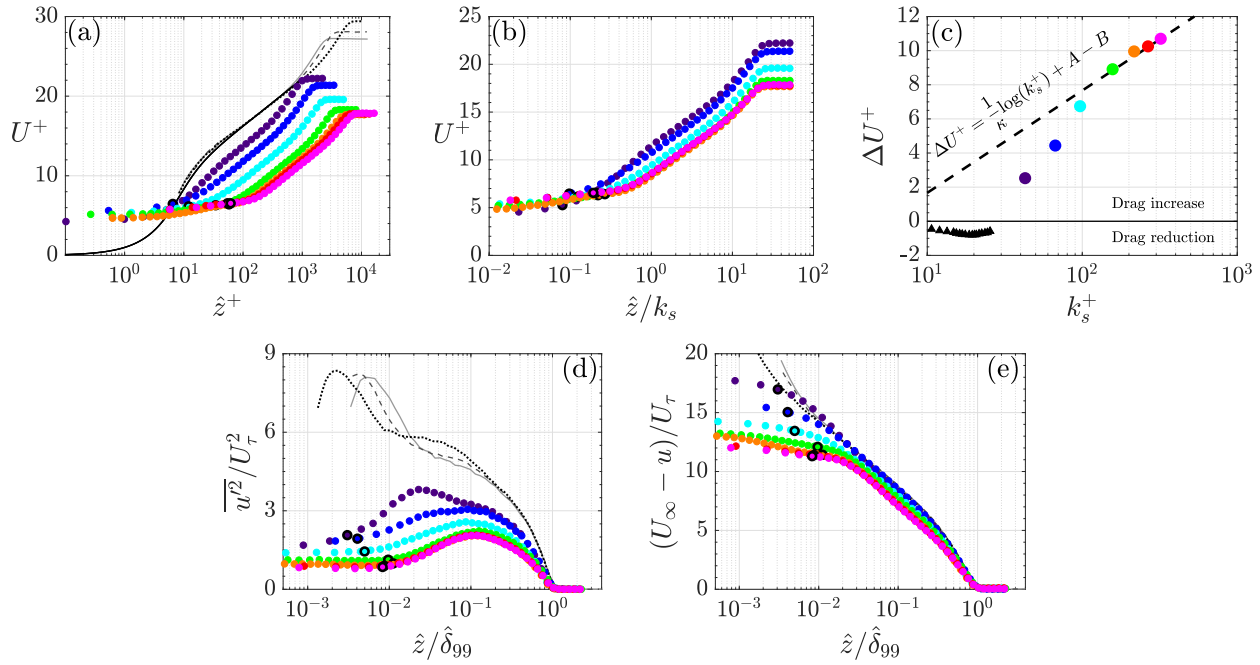

Figure 2: (a) Streamwise velocity profile in viscous units. (b) Streamwise velocity profile in viscous units vs. wall normal distance normalised by the sandgrain roughness. (c) Hama roughness function vs. the sandgrain roughness in viscous units. (d) Turbulence intensity plotted against $\hat{z}/\hat{\delta}_{99}$. (e) Outer layer defect plotted against $\hat{z}/\hat{\delta}_{99}$. ▲ 30° sawtooth riblet data from Bechert *et al.* (1997) [5]. Smooth data from Mathis *et al.* (2011) [12]: — $Re_\tau = 2800$, - - $Re_\tau = 3900$, ···· $Re_\tau = 7300$. ○ Position of the riblet crests for each respective s^+ case. ● $s^+ = 39.8$, ● $s^+ = 62.3$, ● $s^+ = 90.1$, ● $s^+ = 146.0$, ● $s^+ = 201.0$, ● $s^+ = 247.0$, ● $s^+ = 298.3$.

Turbulence intensity and velocity defect

Figure 2(d) shows the viscous-scaled turbulence intensity and figure 2(e) shows the velocity defect as functions of the outer-scaled wall-normal distance ($\hat{z}/\hat{\delta}_{99}$). Under Townsend's outer-layer similarity hypothesis we might expect a collapse in both of these quantities for $\hat{z}/\hat{\delta}_{99} > 0.5$ (e.g. Squire *et al.* 2016 [14]).

Though the velocity defect profile exhibits some collapse, particularly at high Re_τ, the collapse in the turbulence intensity is less apparent. Indeed, although the highest s^+ cases seem to show collapse with each other, they have collapsed to a curve that is very different to the smooth wall data, indicating a departure from Townsend's outer-layer similarity. This departure cannot be completely attributed to erroneous values of U_τ, as it would seem that the high s^+ predictions of U_τ may indeed be fairly accurate, due to their strong similarity with one another. This was verified by calculating U_τ, ΔU^+ and ε by forcing outer-layer similarity. The resulting plots were non-monotonic and clearly erroneous, meaning therefore that at this stage, the more likely explanation is that outer-layer similarity may not exist for this riblet. The velocity defect plot shown in 2(e) displays a monotonically reducing defect (or increasing velocity) within the riblet valley as s^+ increases, up to the appearance of fully rough behaviour.

Looking more closely at the variance plot of figure 2(d), we see a clear reduction in the peak intensity with s^+, as the turbulence intensity reduces from 3.80 at $s^+ = 39.8$ to 2.06 at $s^+ = 201.0 - 298.3$. At $s^+ = 39.8$ the trend is quite similar to a smooth wall with the peak at $\hat{z}/\hat{\delta}_{99} \approx 0.03$. However from $s^+ = 62.3$ onwards, there is no longer a pronounced near-wall peak, with the variance instead exhibiting a peak at $\hat{z}/\hat{\delta}_{99} \approx 0.1$, the magnitude of which diminishes as a function of s^+ before reaching the fully rough state. The turbulence intensity at the riblet crests and below in the valley is also diminishing with increasing s^+, up until the collapse beyond $s^+ = 201.0$. This opposes the Choi *et al.* [7] hypothesis, which attributes the breakdown of the drag reduction to the increased lodgement of turbulence within the riblet valleys. At this stage, we believe that the universal reduction in viscous-scaled energy cannot merely be explained by the increasing U_τ with s^+, although this will be confirmed with further measurements at matched l^+.

Spectral analysis

Figure 3 shows the premultiplied energy spectra of the streamwise velocity fluctuations as a function of the wall normal location $\hat{z}^+$ and streamwise wavelength λ_x^+ for $s^+ = 39.8, 62.3, 90.1, 146.0, 201.0$ and 298.3. Colour contours show the energy for the riblet cases, while the line contours show energy for a smooth wall at approximately matched Re_τ. The spectrogram of $s^+ = 247.0$ is excluded from figure 3 as inline with the expectations of fully rough behaviour, the spectrogram is indistinguishable from that of $s^+ = 201.0$ and $s^+ = 298.3$.

The first observation from figure 3 is that there is a noticeable reduction in energy over the riblets across the entire boundary layer and across all scales as s^+ increases. Most noticeably there is no clear sign of increased energy close to the K–H wavelength ($\lambda_x^+ \approx 150$) for the high s^+ cases in figure 3. Secondly, it is noted that the large scales ($\lambda_x^+ > 1000$) no longer maintain a footprint onto the wall as s^+ increases, but retain a band of energy along the line $\lambda_x^+ = 10\hat{z}^+$ in the higher Re_τ cases. Both of these results are in clear contrast to the smooth wall spectra, and also indicate that contrary to the two proposed hypotheses, at high s^+ it is neither the K–H instability nor the lodgement of near-wall turbulence within the riblet valleys that contribute to the growing ΔU^+ post breakdown.

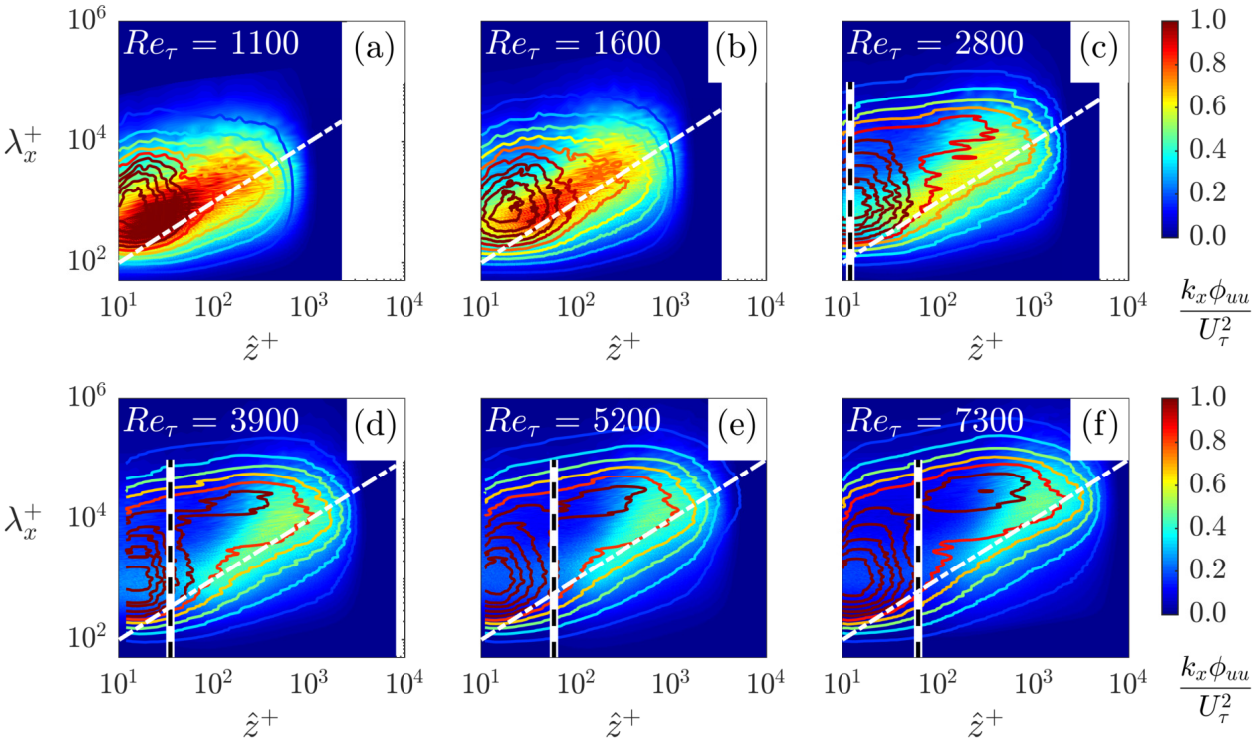

Figure 3: Smooth and riblet wall premultiplied spectrograms of the streamwise energy at approximately matched Re_τ, for (a) $s^+ = 39.8$, (b) $s^+ = 62.3$, (c) $s^+ = 90.1$, (d) $s^+ = 146.0$, (e) $s^+ = 201.0$ and (f) $s^+ = 298.3$. Line contours correspond to the smooth wall, where $Re_\tau = 1100$ and $Re_\tau = 1600$ (interpolated) are from experimental data, but $Re_\tau = 2800$, $Re_\tau = 3900$, $Re_\tau = 5200$ (interpolated) and $Re_\tau = 7300$ are from [12]). **- -** Position of the riblet crests for each s^+ case. The white dot-dash lines show the relationship $\lambda_x^+ = 10\hat{z}^+$.

Conclusion

Results such as 2(d) and 3 show that within the range of $39.8 \leq s^+ \leq 298.3$, there is limited evidence of quasi-streamwise vortices falling into the grooves as the measured turbulence below the riblet crests is seen to reduce as s^+ is increased. The energy associated with the K–H instability also appears to diminish with increasing s^+ (figure 3). However, an approach to fully rough behaviour is undoubtedly seen, even in the absence of pressure drag, which hypothetically may be caused by time-invariant secondary flows that extend from the riblet tips and corners of the riblet valleys.

References

[1] M. Gad-El-Hak. Compliant coatings: A decade of progress. *Appl. Mech. Rev.*, 49:147–157, 1996.

[2] Statista. Number of scheduled passengers boarded by the global airline industry from 2004 to 2018, 2018.

[3] International Air Transport Association. IATA forecasts passenger demand to double over 20 years, 2016.

[4] M. J. Walsh. Turbulent boundary layer drag reduction using riblets. *AIAA 20th Aerospace Sciences Meeting*, 1982.

[5] D. W. Bechert, M. Bruse, W. Hage, J. G. T. van der Hoeven, and G. Hoppe. Experiments on drag-reducing surfaces and their optimization with an adjustable geometry. *J. Fluid Mech.*, 338:59–87, 1997.

[6] P. R. Spalart and J. D. McLean. Drag reduction: enticing turbulence, and then an industry. *Phil. Trans. R. Soc. A*, 369:1556–1569, 2011.

[7] H. Choi, P. Moin, and J. Kim. Direct numerical simulation of turbulent flow over riblets. *J. Fluid Mech.*, 255:1–503, 1993.

[8] P. Luchini, F. Manzo, and A. Pozzi. Resistance of a grooved surface to parallel flow and cross-flow. *J. Fluid Mech.*, 228:87–109, 1991.

[9] R. García-Mayoral and J. Jiménez. Hydrodynamic stability and breakdown of the viscous regime over riblets. *J. Fluid Mech.*, 678:317–347, 2011.

[10] S. Leonardi, P. Orlandi, and R. A. Antonia. Properties of *d*-type and *k*-type roughness in a turbulent channel flow. *Phys. Fluids*, 19, 2007.

[11] N. Hutchins, T. B. Nickels, I. Marusic, and M. S. Chong. Hotwire spatial resolution issues in wallbounded turbulence. *J. Fluid Mech.*, 635:103–136, 2009.

[12] R. Mathis, N. Hutchins, and I. Marusic. A predictive innerouter model for streamwise turbulence statistics in wall-bounded flows. *J. Fluid Mech.*, 681:537–566, 2011.

[13] D. I. Pullin, N. Hutchins, and D. Chung. Turbulent flow over a long flat plate with uniform roughness. *Phys. Fluids*, 2, 082601(R), 2017.

[14] D. T. Squire, C. Morrill-Winter, N. Hutchins, M. P. Schultz, J. C. Klewicki, and I. Marusic. Comparison of turbulent boundary layers over smooth and rough surfaces up to high Reynolds numbers. *J. Fluid Mech.*, 795:210–240, 2016.

[15] J. Nikuradse. Laws of flows in rough pipes. NACA-TM-12, 1933.